



Enhanced photocatalytic activity of annealed polycarbazole-tin oxide nanocomposite against RhB and MB dyes under UV and natural sunlight irradiations

M. Mubarak Ali¹ · D. John Williams¹ · M. Sherin Banu²

Received: 22 January 2020 / Accepted: 20 May 2020 / Published online: 20 October 2020
© The Polymer Society, Taipei 2020

Abstract

The pristine polycarbazole (PCz) and polycarbazole (PCz) -tin oxide (SnO₂) nanocomposite (PCT) were synthesized via facile in-situ polymerization method and analyzed by various advanced techniques. The crystal structure is identified by PXRD and disclosed the primitive tetragonal structure of SnO₂. The annealed PCT exhibited uniform spherical like morphology with low degree of aggregation. The HRTEM analysis confirmed the presence of nanocomposite with the particle size of 7.6 nm for the annealed PCT. The surface area measured from the BET analysis for the annealed PCT is 7.9 m²/g which is 1.9 and 1.6 times higher than the PCz and unannealed PCT respectively. The TG-DTA study revealed the high thermal stability of the annealed material which is 4.8 times higher than the unannealed. The annealed PCT showed higher photocatalytic activity towards rhodamine B (RhB) and methylene blue (MB) dyes under natural sunlight than the UV light under same conditions. Besides, it shows excellent photocatalytic stability after 4 cycles. The extent of degradation is investigated by total organic carbon (TOC) analysis and found that the removal percentage towards the RhB and MB dyes under natural sunlight were 74.16 and 88.16% which is 1.7 and 1.5 times higher than the UV light under same conditions. The practical feasibility of PCT towards the real life time sample is investigated by chemical oxygen demand (COD) technique which is demonstrated a high removal percentage of 50% within 240 min. Thus, the synthesized nanocomposite is inexpensive, reliable and efficient photocatalyst for the removal of textile dyes.

Keywords SnO₂ · Photo catalyst · Polymer nanocomposite · Degradation

Introduction

Dyes are extensively used by various industries such as paper, textile, food, leather and cosmetics. These industries use large amount of dyes every year. It is evaluated that around 10–20% of the dyes were discharged as waste in the water resources during the dyeing and manufacturing process which are carcinogenic in nature and causes serious threat to the human

beings, the hydrosphere and other living organisms in the environment [1]. The major challenge associated with the waste water is the color removal because it is highly complex and difficult to remove. Even a trace of the dye has high visibility which decreased the light penetration and resulted in the reduced photosynthetic process [2]. Hence, it is a challenge for the researchers to remove the dyes from the waste water for the sustainable development of the ecosystem and the environment.

To date, several conventional waste water treatment techniques such as ion-exchange [3], membrane filtration [4, 5], electrolytic treatment [6], electrochemical treatment [7] etc., were employed to remove the pollutants from water. However, these techniques are inefficient, expensive and leave secondary wastes which are very hard to remove. Recently, the photocatalytic technique has been considered as an innovative technique for the waste water remediation by utilizing UV, visible and natural sunlight irradiation due to its fascinating properties such as cheap, high efficiency and reliable [8]. Recently, the conducting polymer nanocomposite

Electronic supplementary material The online version of this article (<https://doi.org/10.1007/s10965-020-02165-7>) contains supplementary material, which is available to authorized users.

✉ M. Mubarak Ali
mubarakscience@gmail.com

¹ Department of Chemistry, Chikkaiah Naicker College, Erode, Tamil Nadu 638004, India

² Department of Chemistry, Government Arts College (A), Salem, Tamil Nadu 636007, India

based photo catalyst has drawn significant attention due to its remarkable optical properties, high separation ability, porosity, recycling ability etc., Several conducting polymer nanocomposites were synthesized by researchers and focused for the degradation of various dyes. However, there is no detailed report on the photo catalytic applications of PCz/SnO₂ nanocomposite so far up to the knowledge of the authors. Hence, we have attempted to synthesize the PCz/SnO₂ nanocomposite and focused our attention on the photocatalytic activity. Recently, the porous crystalline materials were emerged as promising materials for light harvesting and photocatalysis applications due to its exceptional photophysical and electric properties. Among them, the carbazole units has attracted a significant interest for the removal of organic pollutants. It gained wide attention from the researchers for its outstanding properties such as cheap, low band gap and high electrical conductivity. Moreover, the electrical and the optical properties can be tuned easily by substituting the various substituents at the nitrogen atom and at bridged biphenyl units [9–14]. In addition to this, the photocatalytic activity of PCz decorated titanium dioxide (TiO₂) [15], camphor sulphonic acid doped polycarbazole/graphitic carbon nitride (g-C₃N₄) [16] and polycarbazole (PCz)/cuprous oxide (Cu₂O) nanocubes [17] were shown high degradation efficiency over various dyes under various light sources. The SnO₂ is an interesting metal oxide of n-type semiconductor with a wide band gap of $E_g = 3.8$ eV. It is attracted for its outstanding properties such as non-toxic, chemical stability, biocompatible, resistance to acids and alkalis. It is extensively used in diverse field such as chemical sensors, photo electrode in solar cells and mostly used as a catalyst in many photochemical reactions. In addition to this, the photo catalytic activity of magnetic nanocomposite with metalloporphyrin sulfated tin oxide (Fe₃O₄/SnO₂/SO₄²⁻-Co-TPyP-99) [18] and biotemplate SnO₂ intercalated PANI [19] were exhibited excellent activity over various dyes under various light sources.

The main objective of the present work is to synthesize the efficient photocatalyst (PCT) for the degradation of RhB and MB dyes (target pollutants) with real life time sample under UV and natural sunlight irradiation. Comprehensive studies on the effect of annealing on the material properties were investigated. The functional groups of the material are determined by fourier transform infrared (FTIR) technique and its surface morphological structures are analysed by the scanning electron microscope (SEM), high resolution scanning electron microscope (HR-SEM) and high resolution transmission electron microscope-selective area electron diffraction (HRTEM-SAED) techniques. The energy dispersive x-ray spectrometer (EDX) is used to detect the presence of elements. The powder x-ray diffraction technique (PXRD) is used to identify the crystal structure. The surface area, pore size and pore diameter are determined by the brunauer emmett teller (BET) analysis. The Thermal stability is analyzed by using the

thermogravimetric-differential thermal analysis (TG-DTA) technique. The extent of degradation and mineralization were studied by using total organic carbon (TOC) and chemical oxygen demand (COD) technique.

Experimental

Materials

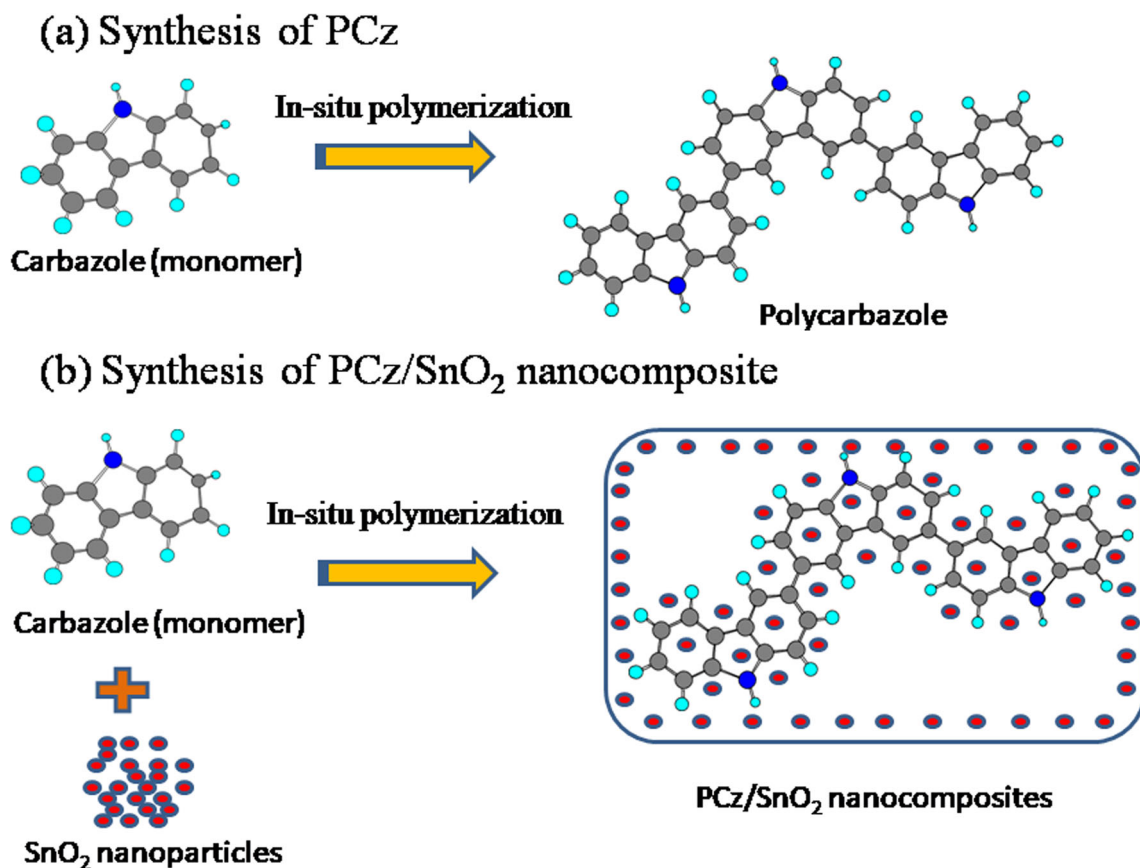
Carbazole monomer, tin dioxide (SnO₂), RhB and MB dyes were purchased from merck, methanol and ammonium peroxydisulfate (APS) from S D Fine-Chem., India and acetone from Sigma-Aldrich.

Synthesis of polycarbazole and polycarbazole-SnO₂ nanocomposites

The PCz/SnO₂ nanocomposites with various compositions were synthesized via in situ oxidative polymerization by using ammonium per sulphate (APS) as an oxidizing agent. The various amounts of SnO₂ in acetone are ultrasonicated for 1 h and drop wise added to the solutions of carbazole dissolved in acetone. These solutions are vigorously stirred for 4 h in order to properly adsorb the carbazole monomers on SnO₂ nanoparticles. These are treated with the solutions of APS in drop wise manner with constant stirring for a period of 24 h at room temperature (30 ± 5 °C). This led to the polymerization of carbazole in which the SnO₂ nanoparticles are adsorbed which resulted in the creamy colored precipitates. The solid material thus obtained is filtered, washed with methanol in order to remove the unreacted ammonium per sulfate and other impurities. The prepared materials are dried at 80 °C for 12 h in an air oven, ground into fine powders and used for further characterization. The sample with various composition are labeled as PCT1 (1:1), PCT2 (1:2), PCT3 (2:1) and PCT4 (4:1). PCz has been synthesized in the same manner without the addition of SnO₂. A comparative study on the effect of annealing on the properties of the material is investigated. The PCT1 is annealed in the oxygen atmosphere at two various temperatures and time. The PCT1 is annealed at 200 °C for 30 h (PCT5) and 400 °C for 40 h (PCT6). (The conditions for the synthesis of PCz and various PCz/SnO₂ nanocomposites were shown in Table. S1 (supplementary files) A schematic representation of the synthesis process of the material is shown in Scheme 1.

Conversion & yields of reactions

Conversion of a reaction is defined as the amount of the reactant consumed or converted into products. Total conversion is determined by the following equation.



Scheme 1 Schematic representation of the synthesis of (a) PCz (b) PCz/SnO₂ nanocomposites

$$\text{Total conversion} = \frac{\text{Practical solid content}}{\text{Theoretical solid content}} \quad (1)$$

The yield of the reaction is defined as the amount of a particular useful product formed in the chemical reaction. It is often compared with the theoretical calculations. When the maximum theoretical amount is calculated as percentage, it is called as percentage yield. Yield of the reaction is determined by the following equation.

$$\text{Yield} = \frac{\text{Weight of the final washed dried powder}}{\text{Weight of the initial components except water}} \quad (2)$$

The total conversion and the yield of the reaction are calculated by using the above equation.

Characterization of polycarbazole-SnO₂ nanocomposite

The functional groups of the material is identified by FTIR spectrophotometer (Perkine Elmer, USA, model Spectrum-BX). The UV absorption spectrum is recorded by using the varian, Cary 5000 instrument. The direct absorption band gap energy of PCT is determined by using the equation given below.

$$\alpha h\nu = C (h\nu - E_g)^2 \quad (3)$$

From the above equation, α = absorption coefficient, C = constant, $h\nu$ = photon energy, E_g = band gap energy.

The crystal structure of the material is investigated by using Bruker AXS D8 Advance X-ray diffractometer. The crystallite size (D) is calculated by using the following equation.

$$D = \frac{K\lambda}{\beta \cos \theta} \quad (4)$$

From the equation, K is the proportionality constant ($k = 0.89$), λ is the wavelength of X-rays (1.5406 \AA for $\text{CuK}\alpha$), β is the full width half maximum (FWHM) of the diffraction peak, and θ is the Bragg diffraction angle and D is the crystallite size.

The particle size is analyzed by Shimadzu SALD-2300 particle size analyzer (PSA). The morphology of the material is performed with scanning electron microscope (JEOL Model JSM - 6390LV), high resolution scanning electron microscopy (Quanta 200 FEG) and the high resolution transmission electron microscope (JEOL 2100 HRTEM at 300 kV). The quanta 200 FEG is used to detect the presence of elements through the energy dispersive x-ray spectrometer (EDX). The surface area, pore size and pore volume is measured by using

BET analysis (Belsorp mini 2). The TGA/DTA of the material is investigated by using Perkin Elmer STA 6000. The total organic carbon (TOC) analysis is carried out by using shimadzu analyzer.

Measurement of photo catalytic activities

The photo catalytic activity of the PCz, PCT1 and PCT6 against RhB and MB dyes were carried out in quartz tubes under UV and natural sunlight irradiation. The parameters for the photocatalytic activity is optimized and the concentrations of RhB is 1×10^{-6} M at pH = 7 and MB is 1×10^{-5} M at pH = 7. The average solar intensity and the UV light intensity is observed (Lutron UV light meter UV-340A) throughout the photocatalytic experiments are 2350 uW cm^{-2} and 860 uW cm^{-2} . Initially the dye solution is stirred for 30 min in the dark for adsorption-desorption equilibrium and afterwards it is irradiated by various light sources. The percentage of degradation is measured by using Lambert's-Beer law from the following equation,

$$\text{Degradation Percentage (\%)} = \frac{(C_0 - C)}{C_0} \times 100 \quad (5)$$

Where, C_0 is the initial dye concentration of the dye before irradiation, and C is the concentration of dye after time t .

Adsorption kinetics can be expressed by the Langmuir–Hinshelwood (L–H) model. The apparent rate constant is calculated by using the following equation.

$$K_{app} = \ln \frac{C_0}{C} \quad (6)$$

Where, k_{app} is the apparent pseudo-first-order reaction rate constant and t is the reaction time. A plot of $\ln(C_0/C)$ versus t , is drawn, from that the k_{app} is calculated from the slope. C_0 is the concentrations of dyes after adsorption in dark for 30 min, and C_t is the concentration of dyes at the given time t .

The real life time sample (reactive black dye) is collected from the industrial site near Perundurai, Tamilnadu, India for the investigation. The quality of the treated sample is measured by chemical oxygen demand (COD) technique using dichromate reflux method.

Results and discussion

Conversion and yields of reactions

The Table S2 (supplementary file) shows the conversion and yield percentage of PCz & various compositions of PCz/SnO₂ nanocomposites. The results showed that the PCT4 (4:1) observed high yield percentage (92%) due to the polymerization of carbazole whereas, the SnO₂ nanoparticles are only

dispersed in the PCz matrix during the synthesis. On the other hand, the PCT2 achieved high conversion (68.8%) and low yield (77.5%) percentage due to the incompleteness of the reaction. Some amount of the product may be lost during the filtration etc., and the standard deviation of the conversion and yield are 14.4 ± 0.02 and 5.2 ± 0.02 respectively.

FTIR analysis

The FTIR spectrum of PCz and PCz/SnO₂ nanocomposites are shown in Fig. 1. The spectrum of PCz (Fig. 1a) shows two N-H stretching vibration peaks at 3415 and 3045 cm^{-1} . The peaks related to the benzenoid and quinonoid units and were observed at 1597 and 1446 cm^{-1} . The bands appeared at 921 , 851 and 717 cm^{-1} were corresponds to the formation of unsubstituted carbazole, which confirms that the polymerization occurred from 3 to 6th positions of PCz. The results are in good agreement with the earlier literature [20]. In case of PCz/SnO₂ nanocomposites, the N-H stretching vibration peak is slightly shifted to lower wave numbers from the PCz. The peaks correspond to the benzenoid and quinonoid units were shifted to lower wave numbers for PCT2. But in the case of PCT1, PCT3 and PCT4, the shift is towards the higher wave numbers. The transmittance percentage of the nanocomposites decreases with the increase in the amount of loading of PCz. The band for the SnO₂ is observed in the range from 619 to 621 cm^{-1} which corresponds to the anti-symmetric and symmetric vibrations of Sn-O-Sn. The results are in well agreement with the previous studies [21, 22]. The broad peak for SnO₂ is observed at 615 for PCT2 and 620 cm^{-1} for PCT4, which may be the result of interaction of N-H bond of PCz with the oxygen of SnO₂. The results are in well agreement as reported earlier [23–25].

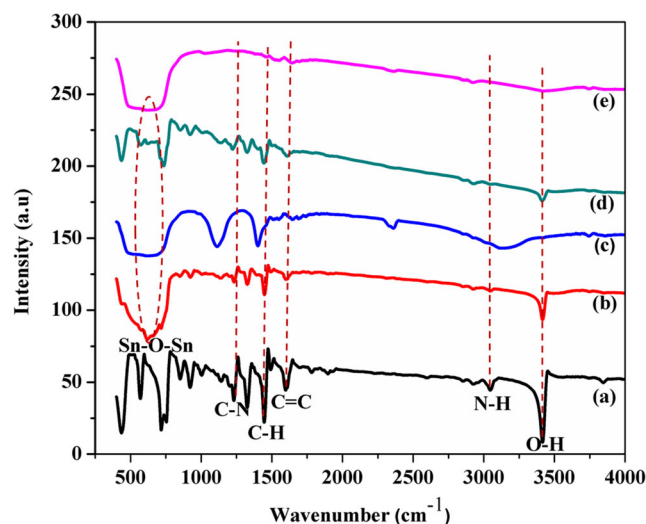


Fig. 1 FTIR spectrum of (a) PCz (b) PCT1 (c) PCT2 (d) PCT3 (e) PCT4

Optical studies

The optical properties of the various PCz/SnO₂ nanocomposites were investigated by UV-vis absorption spectrum and shown in Fig. 2. It shows distinctly red shift and the shifting of the peaks may be due to the π-π* of the benzenoid structure. The characteristic absorption peak of PCT1, PCT2, PCT3 and PCT4 are observed at 335.06, 335.13, 336.64 and 340.74 nm which may be due to the formation of nanocomposite. The band gap values are measured by using the fundamental absorption which is attributed to the electron excitation from the valence band to the conduction band and shown in Fig. S1 (supplementary files). The optical band gap of PCz exhibited a wider band gap of 3.8 eV. Whereas, the optical band gap of PCT1, PCT2, PCT3 and PCT4 are 3.54, 3.54, 3.52 and 3.4 eV respectively. The result indicates that the incorporation of SnO₂ into PCz matrix improve the absorption efficiency in the UV region.

PXRD analysis

The PXRD pattern of the PCz (Fig. 3a) shows peaks at 18.5°, 19.2°, 19.8°, 23.3° and 28°. The pronounced peak observed at 18.5° which is assigned to the PCz backbone. However, the predominant peaks are observed at 26.6°, 33.9°, 51.8° and 66.0° which corresponds to the SnO₂ with preferred orientations of (110), (101), (211), and (301) (Fig. 3b). The 2θ values observed were matched with the standard JCPDS value (JCPDS Card No: 41-1445) of SnO₂ [26]. The planes indicates the FCC crystal structure and the peaks appeared are matched with the primitive tetragonal structure of space group P42/mnm. The pattern for the PCT1 and PCT2 are similar and shown in Fig. 3c and d. It is inferred that the low intense diffraction peaks is appeared for the PCz and the high intense

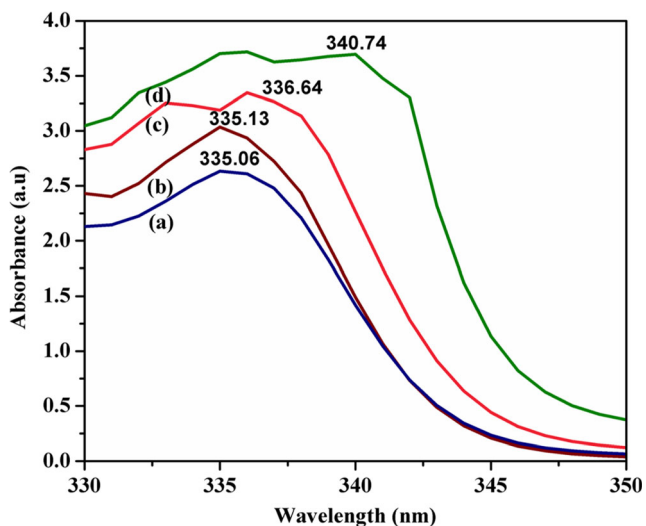


Fig. 2 UV-Vis spectrum of (a) PCT1 (b) PCT2 (c) PCT3 (d) PCT4

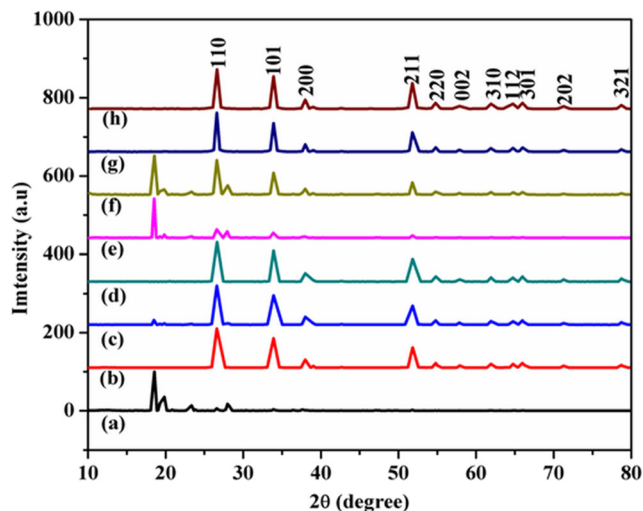


Fig. 3 XRD pattern of (a) PCz (b) SnO₂ (c) PCT1 (d) PCT2 (e) PCT3 (f) PCT4 (g)PCT5 (h) PCT6

peak is observed for SnO₂ which revealed that the crystal structure of SnO₂ is not altered during the synthesis. Moreover, the presence of SnO₂ nanoparticles hinders the crystallization of PCz [27]. As shown in Fig. 3e and f, the PCT3 and PCT4 exhibited high intense peak for PCz and low intense peak for SnO₂ due to the semi crystalline nature of PCz incorporated in the composite which decreased the mass-volume percentage of SnO₂. In addition, the XRD pattern of PCT5 (Fig. 3g) and PCT6 (Fig. 3h) were similar, confirming that there was no significant change in the lattice phase. Whereas, the sharp peaks were observed which indicate good crystallinity [28]. The detailed list of average crystallite size of PCz and various PCz/SnO₂ nanocomposites were shown in Table 1.

Particle size analysis

The particle size of PCT1 is further studied by particle size analysis and shown in Fig. S2a (supplementary file). It is

Table 1 Average crystallite size of PCz, SnO₂ and various PCz/SnO₂ nanocomposites as calculated from XRD patterns using Debye-Scherrer Equation

Material	Crystallite size (nm)	Std deviation
PCz	62.44 nm	12.32
SnO ₂	35.50	10.65
PCT 1	35.40	5.99
PCT 2	31.45	3.98
PCT 3	40.42	3.57
PCT 4	40.70	4.63
PCT 5	23.26	1.74
PCT 6	25.57	2.88

observed that the 25%, 50% and 75% of the particles are present in the size of 134.7 μm , 271.5 μm and 403.3 μm respectively. The average particle size of the material is 271.5 μm and its standard deviation is 0.329. The study revealed that the particles are present as large in size due to agglomeration (particle-particle interaction) and may be present as non-spherical in size. On the other hand, the PCT6 (Fig. S2b) shows that the 25%, 50% and 75% of the particles are in the size of 72 nm, 105 nm and 384.5 μm respectively. Furthermore, the 50% of the particles are present in the nanometer range which is less than the diameter of 100 nm.

Morphological analysis

The Fig. 4 (a–d) depicts the SEM images of PCT1, PCT2, PCT3 and PCT4, which exhibited various morphologies due to the difference in the mass ratio of PCz and SnO_2 nanoparticles. The PCT1 (Fig. 4a) shows highly dense spherical morphology and PCT2 (Fig. 4b) exhibited coral like morphology. Besides, the PCT3 (Fig. 4c) possess nanorod like structure of random particles and PCT4 (Fig. 4d) revealed distorted leaf like morphology. In addition to these, several flocculent structures were seen in the nanocomposites which evidenced the

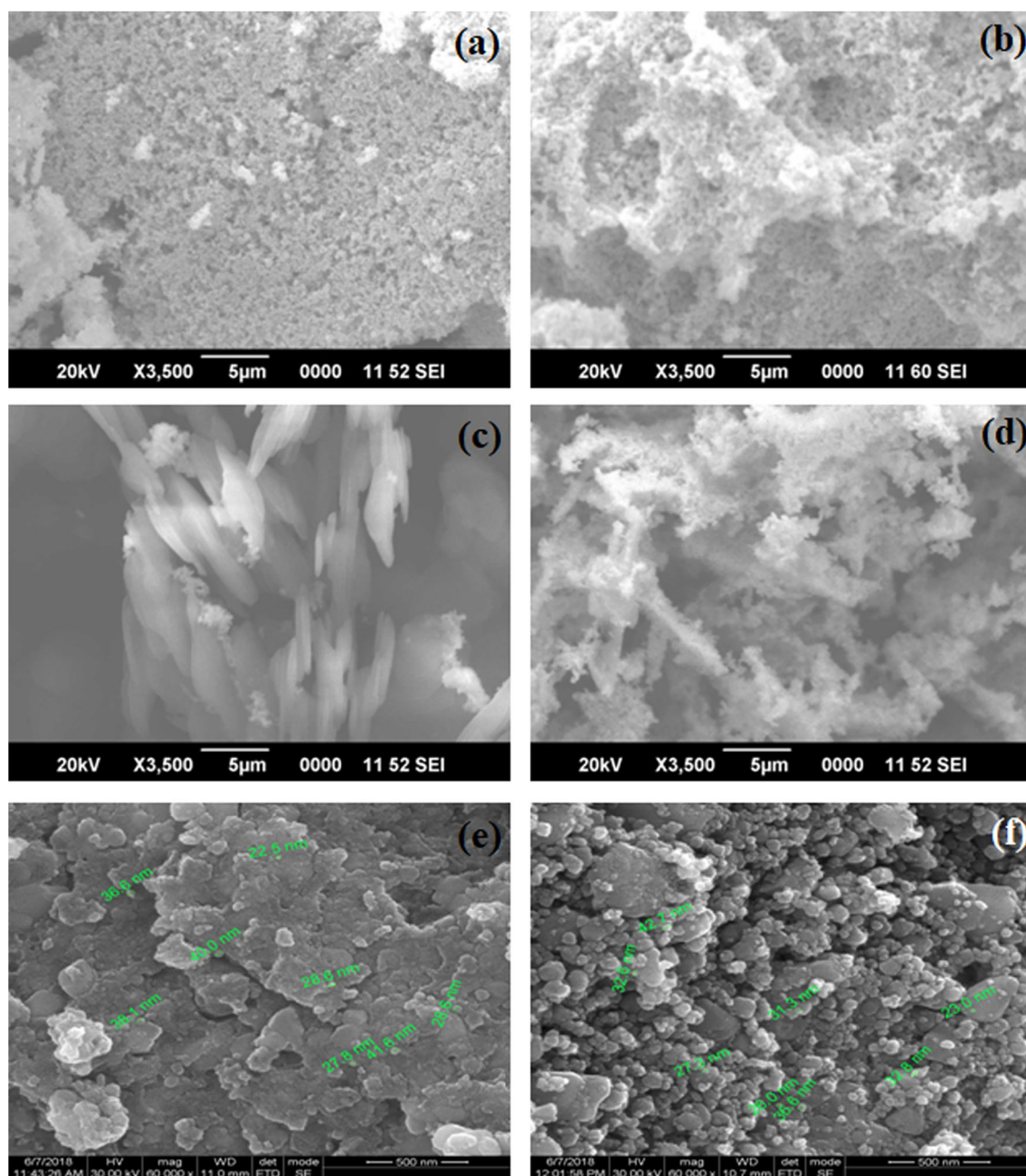


Fig. 4 SEM images of (a) PCT1 (b) PCT2 (c) PCT3 (d) PCT4 (e) PCT5 (f) PCT6

strong interaction between the PCz and SnO₂. The morphology observed for all the nanocomposites shows agglomeration of 100–200 nm. The agglomeration observed may be due to the polarity and electrostatic attraction of SnO₂ nanoparticles. The results are in well agreement as reported earlier [29]. Moreover, the high surface area of the particles leads to agglomeration which reduces the photocatalytic activity. Hence, to reduce the agglomeration of PCT1, it is annealed. As a result, the PCT5 (Fig. 4e) exhibited flakes like structure with less agglomeration rather than PCT1. On the other hand, the PCT6 (Fig. 4f) reveals the uniform spherical like morphology with lower degree of agglomeration than PCT5. The average particle size of PCT5 and PCT6 are 32.9 and 31.5 nm respectively.

The morphology is further investigated by HRTEM technique. The PCT1 exhibited a wide distribution of random (hexagonal and spherical) morphology with the average particle size of 17.78 nm. The aggregated lattice fringes images is observed for PCT1 and shown in Fig. 5b. The SAED pattern of the PCT1 (Fig. 5c) exhibited four diffraction rings and the successive view of the dark and bright fringes showed the polycrystalline nature. The diffraction rings are indexed as the face centered cubic (FCC) structure of SnO₂. The d spacing values obtained from the SAED pattern is 0.38 and 0.21 nm which corresponds to the 110 and 111 plane of SnO₂. The PCT6 (Fig. 5d) shows aggregation due to the π - π and electrovalent interaction

between the PCz and the SnO₂ nanoparticles. The results are in good agreement with the previous studies [19, 30]. The Fig. 5e shows the well resolved lattice fringes images which showed the d spacing values which is well matched with the d spacing value of SnO₂ (JCPDS Card no: 41–1445). The d spacing values are indexed to the d₁₁₀ (0.38 nm) and d₁₀₁ (0.27 nm) plane which is very close to the interplanar distance. The Fig. 5f shows the SAED pattern which represents four successive diffraction rings with high ordered lattice fringes indexed to the face center cubic (FCC).

Elemental analysis

The EDS spectrum of PCT1, PCT2, PCT3 and PCT4 are shown in Fig. 6 (a–d). The peaks are related to tin, oxygen and carbon elements confirmed qualitatively that the material is composed majorly of Sn, C, and O. The sharp peaks reveal that the material is presented mostly as crystalline and the amorphous nature. From the results, the PCT1 exhibited higher atomic (97.16) and weight percentage (93.77) of carbon (C) than the other compositions. However, the PCT3 exhibited higher atomic (22.3) and weight percentage (59.17) of oxygen (O). Similarly the tin (Sn) exhibited higher atomic (73.6) and weight percentage (26.32) than the other compositions.

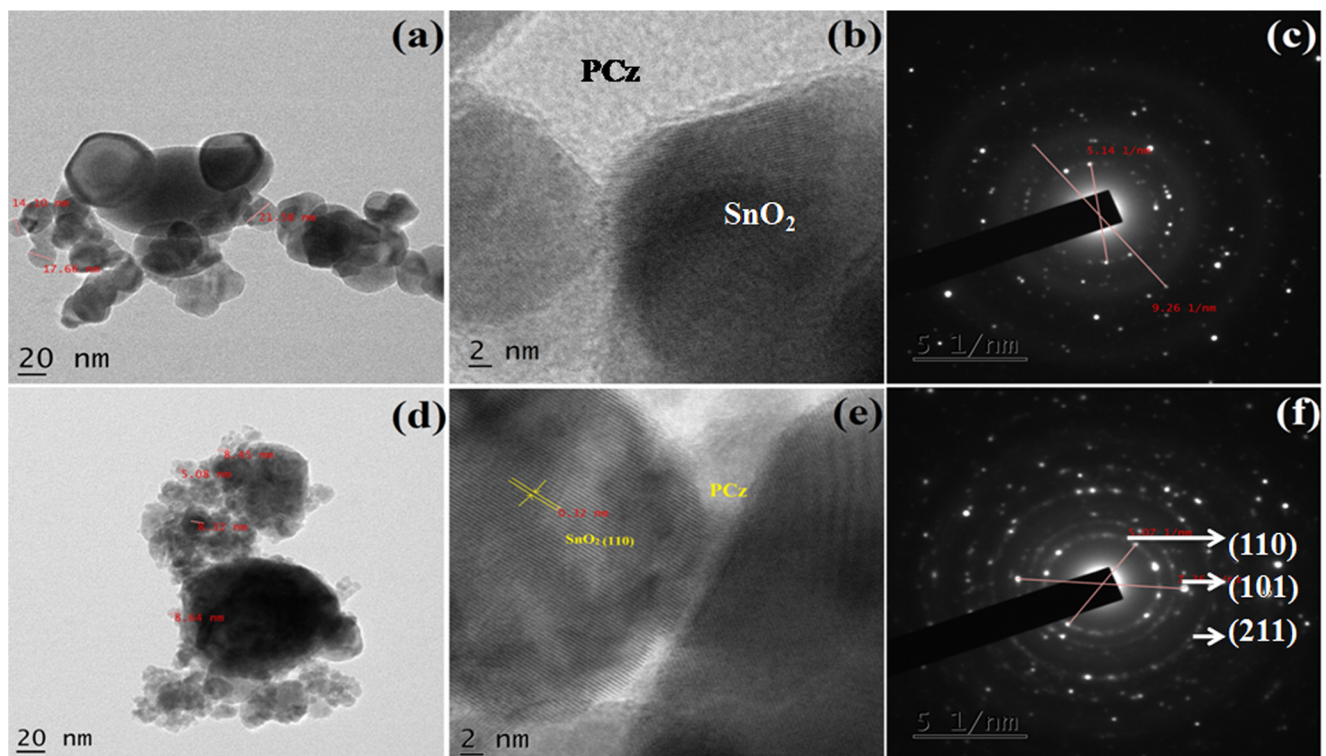


Fig. 5 HRTEM micrographs of (a) PCT1 (b) lattice fringe of PCT1 (c) SAED pattern of PCT1 (d) PCT6 (e) lattice fringe of PCT6 (f) SAED pattern of PCT6

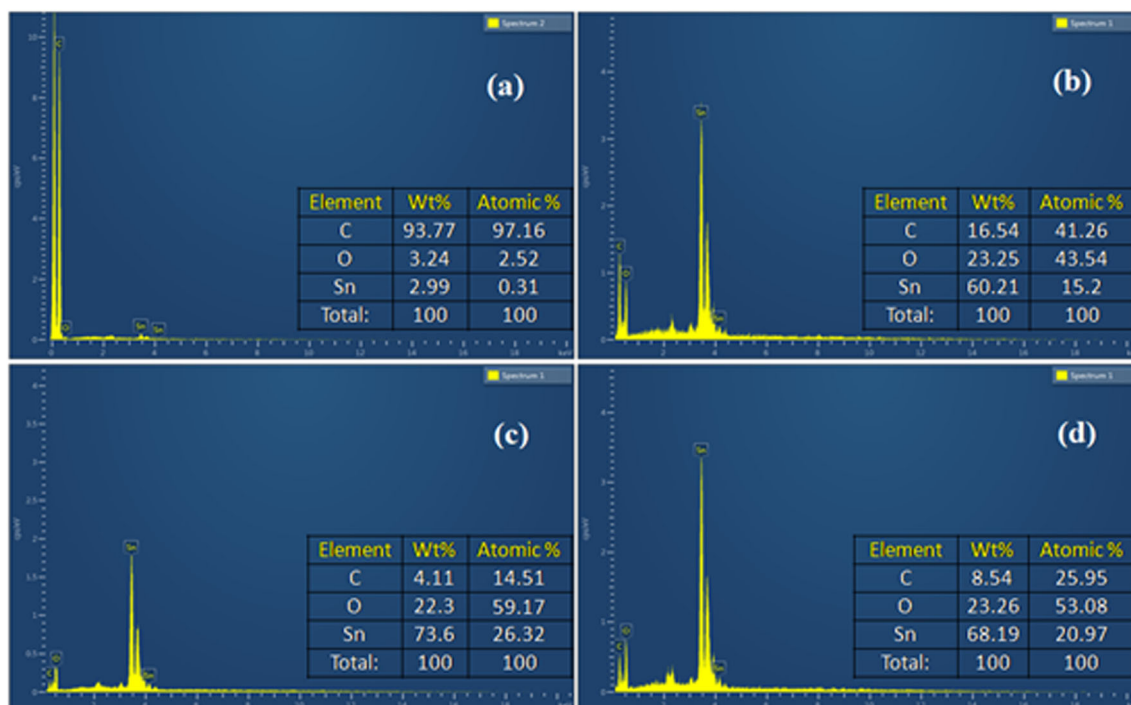


Fig. 6 EDAX of (a) PCT1 (b) PCT2 (c) PCT3 (d) PCT4

BET studies

The surface area and the pore volume are the important factor for enhancing the photocatalytic activity. The surface area, mean pore diameter and pore volume of PCz, PCT1 and PCT6 are summarized in Table S3 (supplementary file). As shown in Fig. S3 (supplementary file) the N_2 adsorption / desorption graph indicates the type I isotherm, suggesting the microporous nature of PCz/ SnO_2 nanocomposites. The nitrogen adsorption capacity of PCz and PCT1 is low which resulted in the small amount of pores in its structure. However, the surface area of PCT6 is $7.9 \text{ m}^2/\text{g}$ and its pore volume is $8.4 \text{ cm}^3/\text{g}$. It is interesting to note that the high surface area of the PCT6 may adsorb more number of dye substances on the surface of the catalyst which is expected to enhance the photocatalytic activity.

Thermal analysis

The thermal stability of the PCz, SnO_2 , PCT1 and PCT5 are investigated by TGA/DTA analysis. The PCz exhibited weight losses at two stages which are shown in the Fig. 7 (a, b). In this case, the first weight loss occurred at $262.66 \text{ }^\circ\text{C}$ and it is estimated to 31.45%. The weight loss is due to the evaporation of physisorbed water molecule and the small polymer chains which is well evidenced by the endothermic peak. The second weight loss

occurred at $702.02 \text{ }^\circ\text{C}$ and it is estimated to 68.55% which is in accordance with the TGA and DTA curve. The SnO_2 nanoparticles show minor weight loss at $339.07 \text{ }^\circ\text{C}$ with the weight loss percentage estimated to 4.5%. On the other hand, the DTA curve of the pure SnO_2 nanoparticles shows no endothermic peak which is evidenced the high thermal stability above $870 \text{ }^\circ\text{C}$.

From the Fig. 7 (a, b), the PCT1 showed the weight loss at three stages. The first one is at $220.68 \text{ }^\circ\text{C}$ which corresponds to the loss of water molecule and the second weight loss is at $642.36 \text{ }^\circ\text{C}$ which is the result of decomposition of polymer (PCz). In addition to these, the weight loss occurred between $40 \text{ }^\circ\text{C}$ to $280 \text{ }^\circ\text{C}$ is due to the oxidation of SnO_2 . The total weight loss estimated is 85.81% at $868.68 \text{ }^\circ\text{C}$ in this case. The result reveals that the PCT1 is subsequently stable above $868.68 \text{ }^\circ\text{C}$ which exhibits high thermal stability than the pristine PCz which is confirmed that the presence of very low concentration of SnO_2 (2.99 wt%). The SnO_2 incorporated in PCT1 leads to high thermal stability. As shown in Fig. 7 (a, b), the PCT 5 has two weight loss regions. In this case, the initial weight loss occurred at $238.41 \text{ }^\circ\text{C}$ is attributed to the loss of water molecule. The second weight loss occurred at $609.08 \text{ }^\circ\text{C}$ which may be the result of decomposition of polymer (PCz). The total weight loss is estimated to 35% at $868.68 \text{ }^\circ\text{C}$. Therefore, the PCT5 exhibited higher thermal stability than the PCz (0% at $702 \text{ }^\circ\text{C}$) and PCT1 (85.81% at $868.68 \text{ }^\circ\text{C}$).

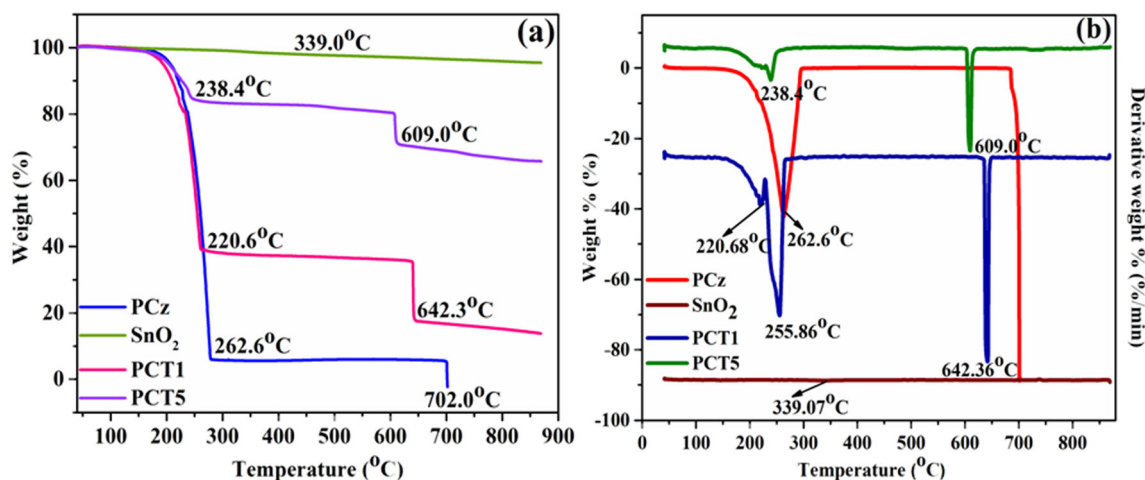


Fig. 7 Combined TGA graph of (a) PCz, SnO₂, PCT1 and PCT5 (b) Combined DTA graph of PCz, SnO₂, PCT1 and PCT5

Evaluation of photo catalytic performance

The photocatalytic activity of the PCz, PCT1 and PCT6 were evaluated against the RhB and MB dyes under dark, UV and natural sunlight irradiation. Initially, the photocatalytic activity of the targeted dyes was performed in the absence of the photocatalyst (PCz, PCT1 and PCT6) under dark conditions, which shows no decomposition after 300 min. However, the degradation efficiency of PCz, PCT1 and PCT6 against RhB dye under dark conditions is 3.07, 5.76 and 26.41%, while it shows 28.15, 35.97 and 39.85% for MB dye under the same conditions. These results show that the photocatalysts (PCz, PCT1 and PCT6) played a crucial role in the photocatalytic activity.

On one hand, the degradation efficiency of PCz over RhB and MB dyes under UV light is 29.88 and 50.32%. In the same way, the PCz degraded 46.31 and 43.44% over RhB and MB dyes under natural sunlight irradiation. It could be found that the low band gap of PCz (3.8 eV) accelerates high electron-hole recombination which decreased the photocatalytic activity. On the other hand, the PCT1 shows the degradation abilities for RhB (68.69%) and MB (85.72%) dyes under UV light irradiation. Similarly, it shows 61.18 and 84.90% for RhB and MB dyes under natural sunlight irradiation respectively. The result indicates that the incorporation of SnO₂ in the PCz matrix played a pivotal role in the degradation of both the dyes under light illumination. This attributes that the PCz matrix not only stabilized the SnO₂ nanoparticles but also reduced the recombination of photogenerated electron-hole pair which facilitated interfacial charge transfer between PCz and SnO₂. Moreover, the surface area and the pore diameter of the PCT1 are higher than the PCz which is also an important factor in determining the degradation efficiency.

The best photocatalytic efficiency was obtained for PCT6 (Fig. 8) over RhB (84.55%) and MB (93.02%) dyes under UV light irradiation, while it shows 95.67 and 99.13% for RhB

and MB dyes under natural sunlight irradiation. On comparing the results of PCT6 with PCT1 and PCz, the degradation efficiency of PCT6 is 1.2 and 2.8 times higher for RhB dye, 2.0 and 1.5 over MB dye than that of PCz and PCT1 under UV light irradiation. In the same way, the PCT6 is 1.0 and 1.8 times increased over RhB dye, 2.0 and 2.2 against MB dye than that of PCz and PCT1 under natural sunlight irradiation. According to the XRD and HRTEM analysis, the crystallinity of PCT6 is increased which reduces the recombination rate of electron-hole pairs. In addition to these, the high surface area of the PCT6 is noted, which is 1.9 and 1.6 times higher than that of PCz and PCT1 which in turn increases the photocatalytic activity. Furthermore, the PCT6 exhibited uniform spherical morphology with lower degree of aggregation which transported the photogenerated charge carriers to induce more electrons for the enhanced photocatalytic activity [31, 32].

The degradation of PCz, PCT1 and PCT6 towards RhB and MB dyes under dark, UV and natural sunlight irradiation with respect to different time intervals was investigated. As shown in figure, the photocatalytic activity of PCz, PCT1 and PCT6 towards RhB and MB dyes under dark conditions is lower which shows that the physical adsorption of the material has some effect on the degradation. However, the photocatalytic ability of PCz, PCT1 and PCT6 under UV and natural sunlight irradiation is higher which indicates that the photocatalytic effect is the key factor in determining the degradation efficiency. Furthermore, the degradation efficiency of PCT1 is higher than PCz. The results suggest that the synergistic effect of PCz and SnO₂ in PCT1 has probably increased the photocatalytic activity. In addition to these, the degradation efficiency of PCT6 is higher than the PCz and PCT1. This is mainly because of the effect of annealing which improved the material properties for the effective separation of photogenerated electron-hole pair for the enhanced photocatalytic activity. The C/Co plots of PCz, PCT1 and PCT6 towards RhB and MB dyes were displayed in Fig. 9 (a–d).

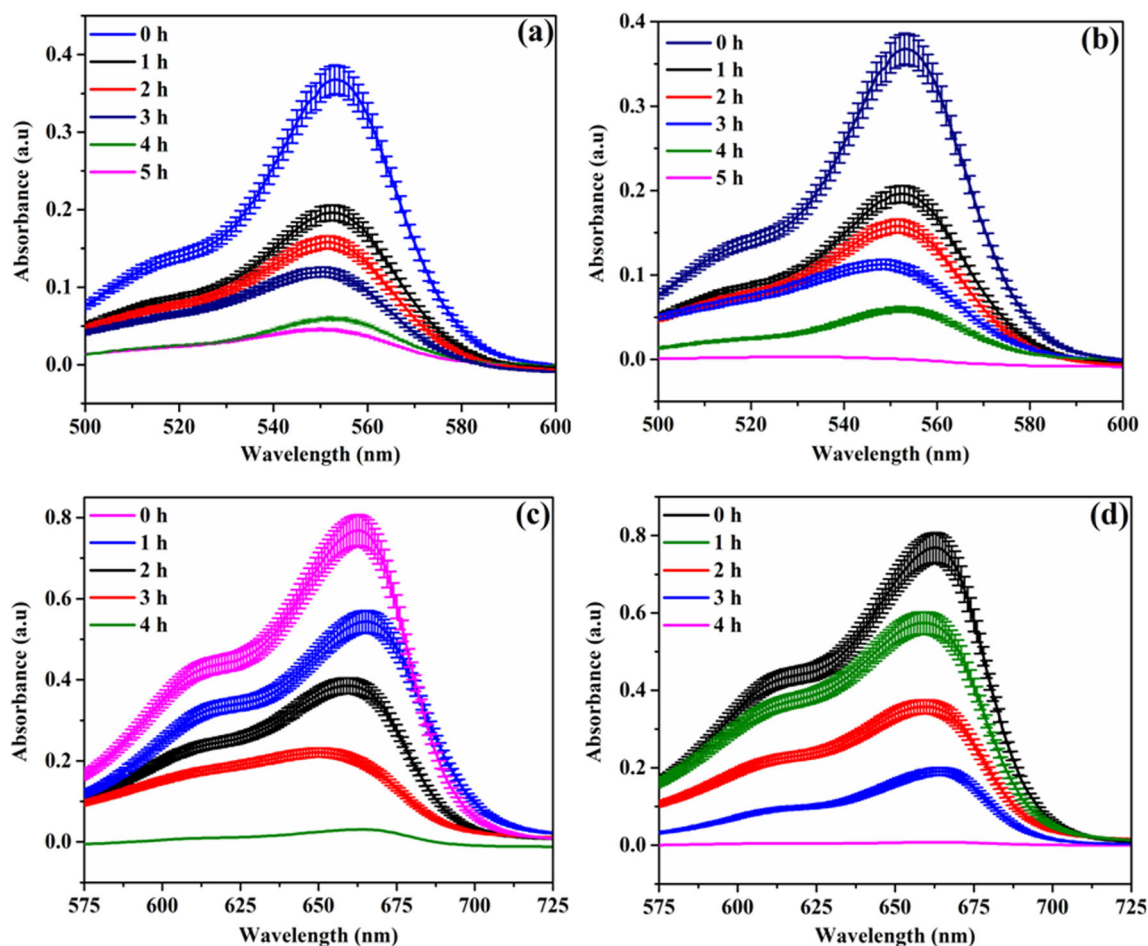


Fig. 8 UV-vis absorption spectrum of PCT6 against various irradiation times under (a) natural sunlight irradiation of RhB (b) UV light irradiation of RhB (c) natural sunlight irradiation of MB (d) UV light irradiation of MB

To scrutinize the photodegradation of RhB and MB dyes, it is fitted and shown in Fig. 10 (a–d). The correlation coefficient (R^2) values of PCT6 towards the degradation of RhB and MB dye under UV and natural sunlight is very close to the 1. Hence, it is evidenced that the PCT6 follows pseudo first order kinetics. The Table 2 summarizes the degradation percentage and numerical rate constant values of PCz, PCT1 and PCT6. The PCT6 exhibits the largest apparent rate constant (9.86×10^{-3}) which is 5.9 and 4.6 times higher than that of PCz and PCT1 over MB dye under natural sunlight. It was found that the degradation of the RhB and MB dyes under natural sunlight is more than the UV light irradiation. The low degradation efficiency under UV light is due to the very low amount of photons (3–5%) produced which resulted in poor photocatalytic activity. Whereas, the natural sunlight produces around 40% of photons which can be utilized for the effective degradation of the dyes. Thus, it is inferred that the dyes can be degraded by employing natural sunlight which is economical, efficient and a promising light source. In order to justify the synthesized material over other photocatalyst, it is compared with the existing literature and summarized in Table 3.

The synthesized PCz/SnO₂ nanocomposite demonstrated high degradation efficiency than the several reported photocatalysts.

The TOC removal percentage of PCT6 against RhB and MB dyes under UV light are 43.19 and 56.31% and natural sunlight is 74.16 and 88.16% respectively. The results demonstrated a high TOC removal under natural sunlight than the UV light which confirms the degradation of the dyes.

It is observed that the photocatalytic activity of MB dye under UV and natural sunlight is more than the RhB dye under same conditions. The low degradation efficiency of RhB dye compared to MB dye may correspond to the large molecular size of RhB dye. Moreover, the photocatalytic activity of the dye is not only depended on the generation of hydroxyl radicals at the interface of the material. It is also depended on the potential of the dye to be adsorbed on the surface of the photocatalyst. Furthermore, the physical and chemical properties of the dyes are different [39–43]. Photocatalytic activity of PCT6 against (a) RhB (b) MB dyes at various time intervals is shown in Fig. S4 (supplementary files).

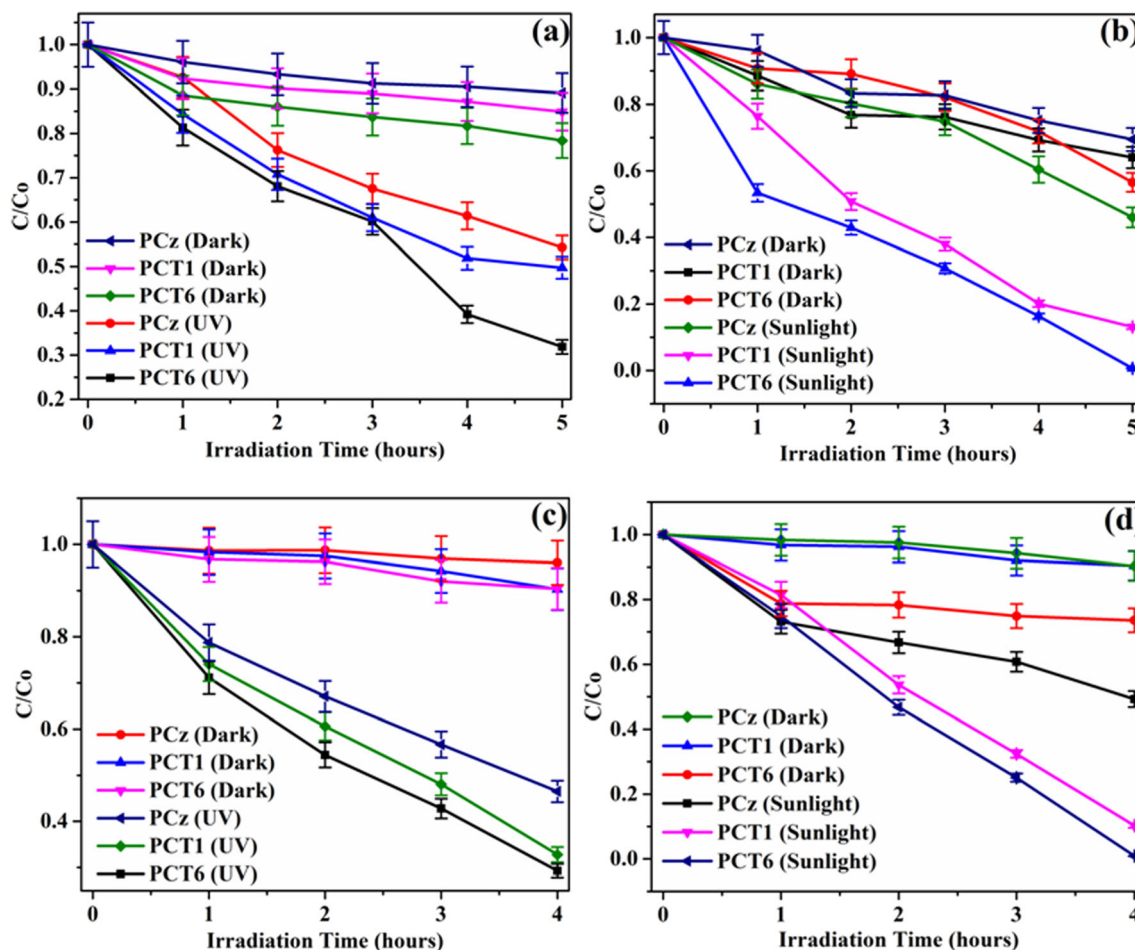


Fig. 9 C/C_0 plots of RhB and MB dyes with respect to time over PCz, PCT1 and PCT6 under (a) UV light irradiation of RhB (b) natural sunlight irradiation of RhB (c) UV light irradiation of MB (d) natural sunlight irradiation of MB

Recycling test

The stability of the material is an important factor for commercial applications. Hence, the degradation of RhB and MB

dyes under UV and natural sunlight are investigated for four consecutive runs and shown in Fig. 11 (a–b). At the first run, the degradation efficiency for PCT6 over RhB dye under UV and natural sunlight is 95.98 and 95.96%. Similarly, it shows

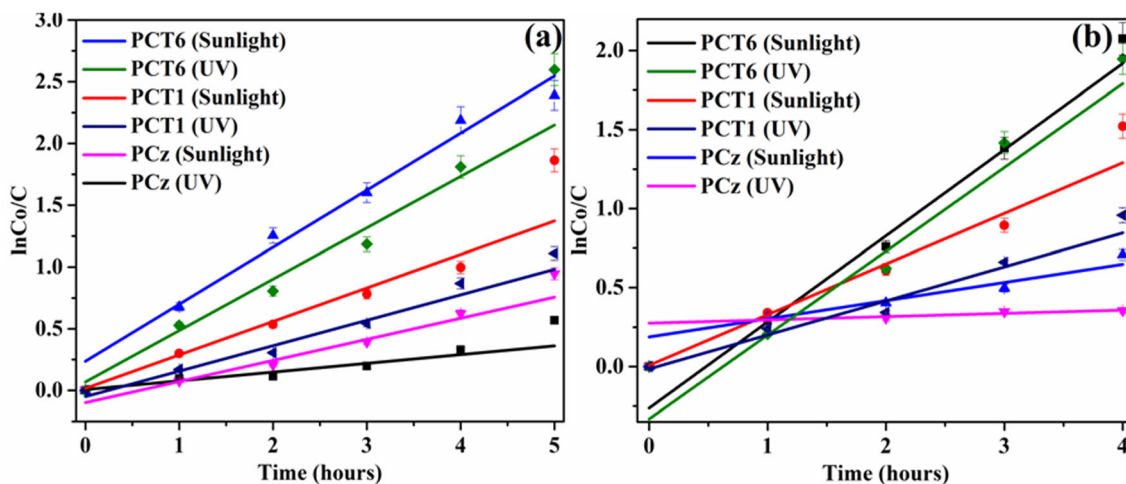


Fig. 10 Comparison of apparent rate constants of PCz, PCT1 and PCT6 towards RhB and MB dyes under UV and natural sunlight irradiation (a) RhB dye and (b) MB dye

Table 2 Degradation % and linear fitting parameters

Catalyst	Dye	Degradation %		Slope		R-Square	
		UV	Sunlight	UV	Sunlight	UV	Sunlight
PCz	RhB	29.88	50.371	5.71×10^{-3}	1.93×10^{-3}	6.28×10^{-1}	8.44×10^{-1}
	MB	46.31	43.44	2.07×10^{-3}	2.13×10^{-3}	8.51×10^{-1}	9.27×10^{-1}
PCT1	RhB	68.69	85.72	3.91×10^{-3}	5.08×10^{-3}	9.43×10^{-1}	8.64×10^{-1}
	MB	61.18	84.90	3.48×10^{-3}	1.67×10^{-3}	3.63×10^{-1}	9.80×10^{-1}
PCT6	RhB	84.55	93.02	2.33×10^{-3}	2.36×10^{-3}	9.01×10^{-1}	9.37×10^{-1}
	MB	95.67	99.13	2.82×10^{-3}	9.86×10^{-3}	8.44×10^{-1}	9.97×10^{-1}

92.64 and 96.26% over MB dye under UV and natural sunlight irradiation. At the fourth run, the degradation rate of RhB dye was still up to 86.82 and 83.48% under UV and natural sunlight irradiation. In the same way, it shows 75.28 and 85.28% after the fourth cyclic run over MB dye under UV and natural sunlight irradiation. The result indicates that the degradation efficiency of PCT6 exhibits a little change; however it maintains the excellent cyclic stability after four runs. The decrease in the degradation efficiency of the used catalyst is due to the accumulation of the degraded products on the surface of the catalyst which hinders the available sites for further reaction. FTIR analysis (Fig. 11c) of the treated and the fresh sample was investigated to explore the stability and the catalytic activity. The result indicates that there is no significant change in the spectrum which indicates that the material is not affected during the repeated cyclic runs. Moreover, the catalyst is not transformed to other organic compound. Furthermore, the XRD (Fig. 11d) of the material employed for the photocatalytic activity indicates that there are no significant changes in the position and intensity, which

confirms that there, is no transformation in the crystal structure as well as in the phase. The results demonstrate that the PCT6 is a potential material possesses strong physical and chemical stability. The recycling ability of PCT6 over MB dye under natural sunlight is shown in Fig. 11.

Possible photocatalytic mechanism

To further explore the photo catalytic activity, a possible mechanism was suggested and evaluated over RhB and MB dyes under UV and natural sunlight irradiation. When the semiconducting material absorbs light (when its energy (hv) is equal to or greater than the semiconductor band gap) it excite the electrons from the valence band (VB) to the conduction band (CB) leaving positive holes in the valence band which resulted in the electron-hole pair (e_{CB}^-/h_{VB}^+) generation.

The semiconducting materials (PCz, PCT1 & PCT6) are irradiated by UV/Sunlight which produces electron-hole pairs.

Table 3 Comparison of the photocatalytic activity of PCT6 over RhB and MB dyes with the reported photocatalyst

S.No	Photocatalyst	Dye	Light source	Degradation (%)	Ref
1	NC/ZnO	RhB	sunlight	76	[33]
2	PANI/TiO ₂	RhB	UV	83.2	[34]
3	PANI/TiO ₂	RhB	Sunlight	67.1	[34]
4	TiO ₂ /rGO	RhB	UV	81	[35]
5	PTh/Al ₂ O ₃	RhB	Sunlight	81.75	[36]
6	PCz/SnO ₂	RhB	UV	84.55	This study
7	PCz/SnO ₂	RhB	Sunlight	93.02	This study
8	PANI/ZnO	MB	UV	79	[37]
9	PANI/ZnO	MB	Sunlight	97	[37]
10	PTh/Al ₂ O ₃	MB	UV	84.73	[36]
11	PTh/Al ₂ O ₃	MB	Sunlight	77.38	[36]
12	PEDOT/MnO ₂	MB	UV	93.3	[38]
13	PEDOT/MnO ₂	MB	sunlight	95.7	[38]
14	PCz/SnO ₂	MB	UV	95.67	This study
15	PCz/SnO ₂	MB	Sunlight	99.13	This study

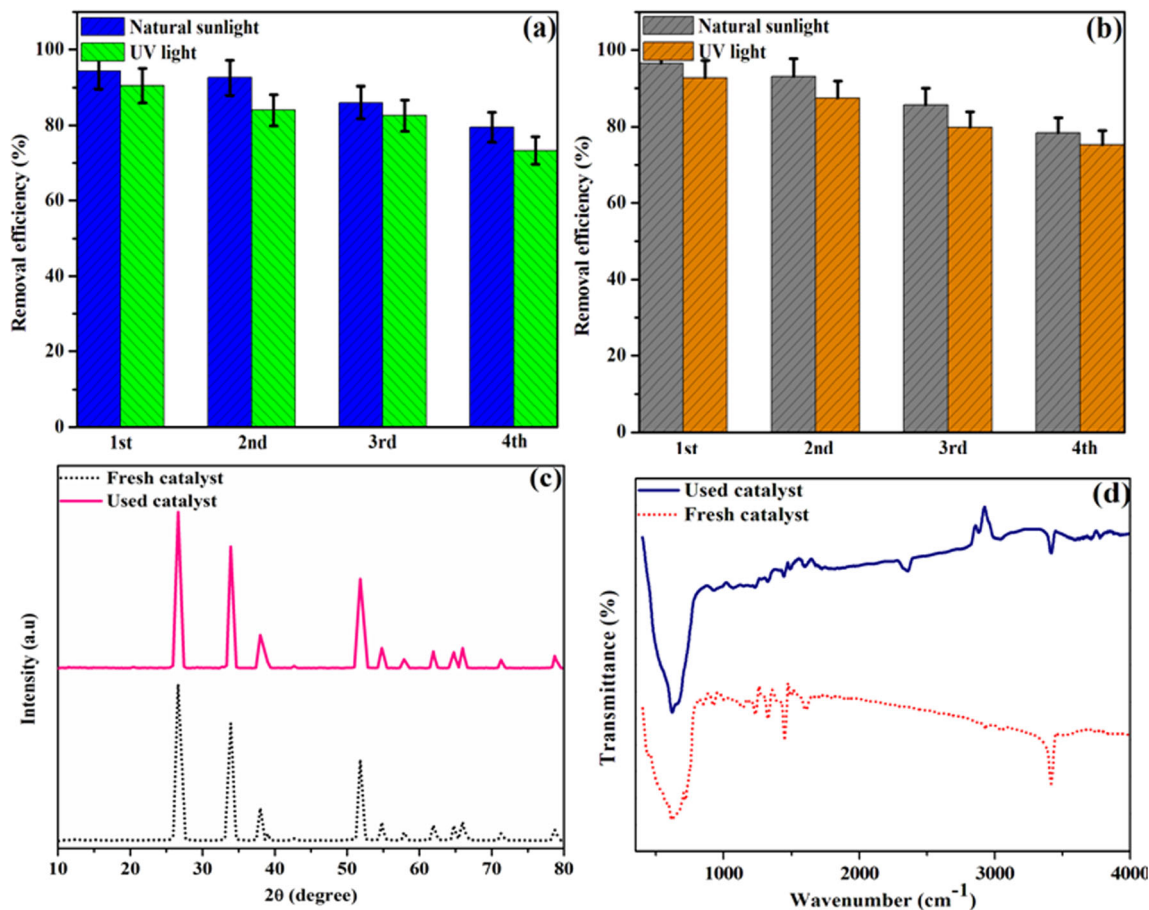
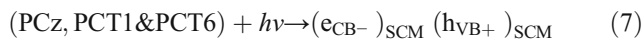
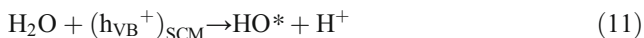
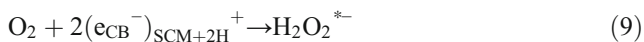


Fig. 11 Recycling ability of PCT6 against (a) RhB dye under UV and natural sunlight irradiation (b) MB dye under UV and natural sunlight irradiation (c) XRD pattern of fresh and used PCT6 (d) FT-IR spectra of fresh and used PCT6

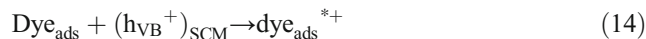
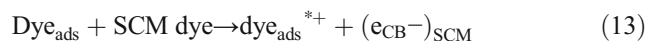


The electron-hole pair after receiving the energy from the UV/Sunlight produces hydroxyl (OH*) and super-oxide (O₂^{*-}) radicals. These radicals are very active and migrated to the catalytic surface to oxidize and mineralize the dyes [44, 45] (Eqs. 8–11). However, the oxidation of the pollutants and the reduction of oxygen do not occur simultaneously. There will be an accumulation of electrons in the conduction band (CB) which increases the rate of recombination of electrons and holes. Hence, the prevention of electron accumulation is necessary for the efficient photocatalytic activity.

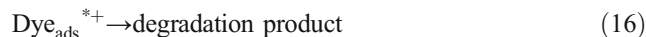
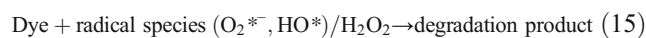


The PCz is a suitable material (narrow band gap) which is used as a sensitizer to improve the efficiency and behaves as a sink for the absorbed photo generated electrons and hinder the recombination of electron-hole pairs which transfers the

electrons from the lowest unoccupied molecular orbital of PCz into the conduction band of SnO₂ in the PCz/SnO₂ nanocomposite. This process is used to reduce the charge carrier which generates more free radicals via interfacial charge transfer (Eqs. 12–14).



The radicals generated is reacted with the respective dyes and mineralize into degraded product which can be identified by the color change occurs in the RhB and MB dyes (Eqs. 15 and 16)



The result evidenced that the PCz and SnO₂ are considered as promising choice for the efficient photocatalytic activity. The combination of PCz and SnO₂ is energetically favorable for the splitting of electron-hole pairs and interfacial charge transfer between PCz and SnO₂. Furthermore, the annealed

PCz/SnO₂ nanocomposite improved the crystallinity, surface properties, surface area and pore diameter, which enhanced the photocatalytic activity. The detailed photocatalytic process of the PCz/SnO₂ nanocomposite has been exhibited in the Fig. S5 (supplementary files).

Real life time sample analysis

The practical feasibility of PCT6 over real life time sample is evaluated by the chemical oxygen demand (COD) technique. The COD test reflects the amount of oxygen required to produce the CO₂ and H₂O during the mineralization of the organic species. The high COD removal of 50% within 240 min is observed for PCT6 which indicates the mineralization of higher organic substance. [46, 47]. The degradation efficiency measured by the UV spectrum after 240 min of photo catalytic treatment is 65%. The degradation efficiency and the COD results indicate the potential of the synthesized material for industrial applications. (The photo catalytic activity of the material against real life time sample under natural sunlight is shown in Fig. S6 (Supplementary files).

Conclusions

The PCz and PCz/SnO₂ nanocomposite were synthesized via in-situ polymerization technique. The FTIR spectrum exhibited well resolved peaks which evidenced the formation of the nanocomposite. The band gap of the material is measured from the tauc plot is 3.54 eV which was suitable for the degradation of dyes under light illumination. The SEM analysis revealed the uniform spherical like morphology for PCT6 with the average particle size of 33 nm. The HRTEM images exhibited the random morphology (spherical and hexagonal) for the PCT1 and aggregated morphology for the PCT6. The total weight loss observed from the TGA analysis for PCz, PCT1 and PCT6 is 0% (702.02 °C), 85.81% (868.68 °C) and 35% (868.68 °C), which shows that the thermal stability of PCT6 is superior to that of PCz and PCT1. The degradation efficiency of PCT6 over RhB and MB dyes under UV light is 84.55 and 95.67% and natural sunlight irradiation is 93.02 and 99.13%. The enhanced photocatalytic activity of PCT6 is related to the high surface area, unique optical, surface properties and the uniformity of the particles. The photo catalytic activity follows pseudo-first order kinetic model. The probable mechanism for the photo catalytic activity confirmed the synergistic effect of the annealed material. The real life time sample analysis revealed that the material is reliable for practical applications. Furthermore, the degradation efficiency of PCT6 is high under natural sunlight than UV irradiation.

Thus, the synthesized PCz/SnO₂ nanocomposite is an efficient photo catalyst for the waste water remediation and other industrial applications.

Acknowledgements The authors gratefully acknowledge the STIC, cochin, for providing the following characterization facilities such as XRD, SEM, TGA-DTA, HR-TEM as well as SAIF, IIT Madras for HR-SEM facility and also thank the Central research lab, Vellalar college of technology, Erode for FTIR, UV studies. One of the author D. John Williams (UGC-RGNFD-2016-17-TAM-2904) express his sincere gratitude to the University Grants Commission (UGC) - Rajiv Gandhi National Fellowship for Disabled (RGNFD) New Delhi, for granting the Junior and Senior Research Fellowship (JRF-SRF).

References

- Zhan Y, Guan X, Ren E, Lin S, Lan J (2019) Fabrication of zeolitic imidazolate framework-8 functional polyarylonitrile nanofibrous mats for dye removal. *J Polym Res* 26:145
- Ju DJ, Byun IG, Park JJ, Lee CH, Ahn GH, Park TJ (2008) Biosorption of a reactive dye (Rhodamine-B) from an aqueous solution using dried biomass of activated sludge. *Bioresour Technol* 99:7971–7975
- Raghu S, Ahmed Basha C (2007) Chemical or electrochemical techniques, followed by ion exchange, for recycle of textile dye waste water. *J Hazard Mater* 149:324–330
- Panda SR, De S (2015) Performance evaluation of two stage nanofiltration for treatment of textile effluent containing reactive dyes. *J Environ Chem Eng* 3:1678–1690
- Avlonitis SA, Poullos I, Sotiriou D, Pappas M, Moutesidis K (2008) Simulated cotton dye effluents treatment and reuse by nanofiltration. *Desalination* 221:259–267
- He P, Wang L, Xue J, Cao Z (2010) Electrolytic treatment of methyl orange in aqueous solution using three-dimensional electrode reactor coupling ultrasonics. *Environ Technol* 31:417–422
- Shen ZM, Wu D, Yang J, Yuan T, Wang WH, Jia JP (2006) Methods to improve electrochemical treatment effect of dye waste water. *J Hazard Mater* 131:90–97
- Khaled Ossoss M, Hassan ER, Ayman Al-Hussaini S (2019) Novel Fe₂O₃@PANI-o-PDA core-shell nanocomposites for photocatalytic degradation of aromatic dyes. *J Polym Res* 26:199
- Raj V, Madheswari D, Ali MM (2010) Chemical formation, characterization and properties of polycarbazole. *J Appl Polym Sci* 116: 147–154
- Ahmed El-Mahdy FM, Liu T-E, Kuo S-W (2020) Direct synthesis of nitrogen doped mesoporous carbons from triazine functionalized resol for CO₂ uptake and highly efficient removal of dyes. *J Hazard Mater* 391:122163
- Ahmed El-Mahdy FM, Kuo C-H, Alshehri AM, Young C, Yamauchi Y, Kim J, Kuo S-W (2018) Strategic design of triphenylamine and triphenyltriazine-based two dimensional covalent organic frameworks for CO₂ uptake and energy storage. *J Mater Chem A* 6:19532–19541
- Ahmed El-Mahdy F.M, Christine Young, Jeonghun Kim, Jungmok You, Yusuke Yamauchi, Shiao-Wei Kuo (2019) Hollow microspherical and microtubular [3+3] carbazole-based covalent organic

- frameworks and their gas and energy storage applications. *ACS Appl Mater Interfaces* 11: 9343–9354
13. Mohamed Gamal Mohamed, Ahmed El-Mahdy F M, Mahmoud Ahmed M M, Shiao Wei kuo (2019) Directly synthesized microporous bicarbazole based covalent triazine frameworks for high performance energy storage and carbon dioxide uptake. *Chempluschem* 84:1767–1774
 14. Narendran Rajendran, Jacobsamuel, Mohamed Amin O, Entesar Al-Hetlani, Saad Makhseed (2020) Carbazole-tagged pyridinic microporous network polymer for CO₂ storage and organic dye removal from aqueous solution. *Environ Res* 182:109001
 15. Kashyap J, Ashraf SM, Riaz U (2017) Highly efficient photocatalytic degradation of amido black 10b dye using polycarbazole-decorated TiO₂ nanohybrids. *ACS Omega* 2:8354–8365
 16. P. Praveena, S. Dhanavel, D. Sangamithirai, V. Narayanan, A. Stephen (2018) Visible light driven photocatalytic degradation of methylene blue using novel camphor sulfonic acid doped polycarbazole/g-C₃N₄ nanocomposite. *DAE solid state physics symposium, AIP Conf. Proc.*, 1942:050131–050134
 17. Sun W, Sun W, Zhuo Y, Chu Y (2011) Facile synthesis of Cu₂O nanocube/polycarbazole composites and their high visible-light photocatalytic properties. *J Solid State Chem* 184:1638–1643
 18. Ghafuri H, Mohammadi F, Rahimi R, Mohammadiyan E (2016) Synthesis and characterization of a new magnetic nanocomposite with metalloporphyrin (Co-TPyP) and sulfated tindioxide (Fe₃O₄@SnO₂/SO₄²⁻), and investigation of its photocatalytic effects on degradation of rhodamine b. *RSC Adv* 6:83947–83953
 19. Karpuraranjith M, Thambidurai S (2016) Biotemplate-SnO₂ particles intercalated PANI matrix: enhanced photocatalytic activity for degradation of MB and RY-15 dye. *Polym Degrad Stab* 133:108–118
 20. Macit H, Sen S, Sacat M (2005) Electrochemical synthesis and characterization of polycarbazole. *J Appl Polym Sci* 96:894–898
 21. Fujihara S, Maeda T, Ohgi H, Hosono E, Imai H, Kim SH (2004) Hydrothermal routes to prepare nanocrystalline mesoporous SnO₂ having high thermal stability. *Langmuir*. 20:6476–6481
 22. Xia G, Li N, Li D, Liu R, Wang C, Li Q, Lu X, Spindelov JS, Zhwng J, Wu G (2013) Graphene/Fe₂O₃/SnO₂/ternary nanocomposites as a high performance anode for lithium ion batteries. *ACS Appl Mater Interfaces* 5:8607–8614
 23. Riaz U, Ashraf SM, Khan N (2011) Effects of surfactants on microwave-assisted solid-state intercalation of poly(carbazole) in Bentonite. *JNanopart Res* 13:6321–6331
 24. Tao Y, Zhang K, Zhang Z, Cheng H, Jiao C, Zhao Y, Xu W (2016) Enhanced electrochromic properties of donor-acceptor polymers via TiO₂ composite. *Polymer* 91:98–105
 25. Iram N.e, Khan M S, Jolly R, Arshad M, Alam M, Alam P, Khan R H, Firdaus F (2015) Interaction mode of polycarbazole-titanium dioxide nanocomposite with DNA: molecular docking simulation and in-vitro antimicrobial study. *J Photochem Photobiol, B*, 153: 20–32
 26. Dhanya chandran, Lakshmi nair S, Balachandran B, Rajendra babu K, Deepa M (2016) Band gap narrowing and photocatalytic studies of Nd³⁺ ion-doped SnO₂ nanoparticles using solar energy. *BullMater Sci* 39:27–33
 27. Pang H, Huang C, Chen J, Liu B, Kuang Y, Zhang X (2010) Preparation of polyaniline-tin oxide composites and their application in methanol electro-oxidation. *J Solid State Electrochem* 14: 169–174
 28. Jadoun S, Ashraf SM, Riaz U (2017) Tuning the spectral, thermal and fluoresecent properties of conjugated polymers via random copolymerization of hole transporting monomers. *RSC Adv* 7: 32757–32768
 29. Aminuzzaman M, Pohying L, Goh W-S, Watanabe A (2018) Green synthesis of zinc oxide nanoparticles using aqueous extract of garcinia mangostana fruit pericarp and their photocatalytic activity. *Bull Mater Sci* 41:50–60
 30. Liang J, Wei W, Zhong D, Yang Q, Li L, Lin G (2012) One-step in situ synthesis of SnO₂/Graphene nanocomposite and its application as an anode material for Li-ion batteries. *ACS Appl Mater Interfaces* 4:454–459
 31. Tsai SJ, Cheng S (1997) Effect of TiO₂ crystalline structure in photocatalytic degradation of phenolic contaminants. *Catal Today* 33:227–237
 32. Tanaka K, Capule M, Hisanaga FT (1991) Effect of crystallinity of TiO₂ on its photocatalytic action. *Chem Phys Lett* 187:73–76
 33. Neha tavker, Manu sharma (2018) Enhanced photocatalytic activity of nanocellulose supported zinc oxide composite for RhB dye as well as ciprofloxacin drug under sunlight/visible light. *AIP conference proceedings* 1961:030013–1–030013-8
 34. Gao jinzhang, Li shengying, Yang Wu, Zhao Guohu X, Bo Lili, Song Li (2007) Preparation and photocatalytic activity of PANI/TiO₂ composite film. *Rare metals*, 26:1–7
 35. Gabriela byzynski, Diogo volanti P, Caue ribeiro, Valmor masteraro R, Elson longo (2018) Direct photo-oxidation and superoxide radical as major responsible for dye photodegradation mechanism promoted by TiO₂-rGO heterostructure. *J Mater Sci Mater Electron* 29: 17022–17037
 36. Vijeth Hebri, Ashok kumar S P, Yesappa L, Vandana Molahalli (2019) Photocatalytic degradation of methylene blue and rhodamine b using polythiophene nanocomposites under visible and UV light. *AIP conference proceedings* 2115 (1): 030536–1–030536-4
 37. Eskizeybek V, Sar F, Gulce H, Gulce A, Avc A (2012) Preparation of the new polyaniline/ZnO nanocomposite and its photocatalytic activity for degradation of methylene blue and malachite green dyes under UV and natural sunlight irradiations *Appl. Catal, B* 119:197–206
 38. Zhang L, Jamal R, Zhao Q, Wang M, Abdiryim T (2015) Preparation of PEDOT/GO, PEDOT/MnO₂ and PEDOT/GO/MnO₂ nanocomposites and their application in catalytic degradation of methylene blue. *Nanoscale Res Lett* 10:148–157
 39. Zhou Q, Zhong YH, Chen X, Huang XJ, Wu YC (2014) Mesoporous anatase TiO₂/reduced graphene oxide nanocomposites: a simple template-free synthesis and their high photocatalytic performance. *Mater Res Bull* 51:244–250
 40. Cheng L, Zhang S, Wang Y, Ding G, Jiao Z (2016) Ternary P25–graphene–Fe₃O₄ nanocomposite as a magnetically recyclable hybrid for photodegradation of dyes. *Mater Res Bull* 73:77–83
 41. Wang F, Zhang K (2011) Reduced graphene oxide-TiO₂ nanocomposite with high photocatalytic activity for the degradation of rhodamine b. *J Mol Catal A Chem* 345:101–107
 42. Zhou KF, Zhu YH, Yang XL, Jiang X, Li CZ (2011) Preparation of graphene–TiO₂ composites with enhanced photocatalytic activity, *new J. Chem.* 35:353–359
 43. Nezamzadeh-Ejehieh A, Karimi-Shamsabadi M (2013) Decolorization of a binary azo dyes mixture using CuO incorporated nanozeolite-X as a heterogeneous catalyst and solar irradiation. *Chem Eng J* 228:631–641
 44. Fujishima A, Rao TN, Tryk DA (2000) Titanium dioxide photocatalysis. *J PhotochemPhotobiol C* 1:1–21
 45. Hoffmann MR, Martin ST, Choi W, Bahnemann D (1995) Environmental applications of semiconductor photocatalysis. *Chem Rev* 95:69–96
 46. Wang T, Shi L, Tang J, Malgras V, Asahina S, Liu G, Zhang H, Meng X, Chang K, He J, Terasaki O, Yamauchi Y, Ye J (2016) A

Co₃O₄ embedded porous ZnO rhombic dodecahedron prepared using Zeolitic imidazolate frameworks as precursors for CO₂ photoreduction. *Nanoscale* 8:6712–6720

47. Mohaghegh N, Rahimi E, Gholami MR (2015) Ag₃PO₄/BiPO₄ p-n heterojunction nanocomposite prepared in room temperature ionic

liquid medium with improved photocatalytic activity. *Mater Sci Semicond Process* 39:506–514

Publisher's note Springer Nature remains neutral with regard to jurisdictional claims in published maps and institutional affiliations.